

Comparison Between Theory and Flight Ablation Data¹

HENRY HIDALGO² AND LEO P. KADANOFF³
Avco-Everett Research Laboratory, Everett, Mass.

A theory for ablation of glassy materials under laminar and turbulent heating is verified by using data from an AICBM nose cone that was recovered after flight from a typical 5000-naut mile trajectory. The missile geometry is of the Thor-Able type, and the ablative material on the spherical cap and cone is opaque quartz. Excellent agreement is found between theoretical and experimental results. The actual value for the maximum ablated thickness along the sphere and cone is 9% higher than the theoretical value, whereas the weight loss of ablated material from the spherical nose and cone agree within 20%. The fraction of ablated material which vaporized during re-entry is only 3% higher than the theoretical value. Most of the difference in these results can be explained by the effect of impurity material on the viscosity of opaque quartz.

Nomenclature

A	= body cross-sectional area
C_D	= drag coefficient
c_p	= specific heat at constant pressure
G	= acceleration, g 's
h	= enthalpy
h_v	= heat of vaporization
h_{eff}	= effective energy absorbed per unit mass of ablated material
k	= thermal conductivity
\hat{n}	= refractive index
n	= viscosity law exponent
p	= pressure
P_x	= $p_x + G \sin \theta$
q	= heat transfer rate per unit area
q_0	= aerodynamic heat transfer rate per unit area to a hot, nonablating wall
q_r	= $\epsilon \sigma T_w^4$
r	= body dimension normal to body axis of symmetry
R_{eff}	= effective reflectivity of surface
t	= time
T	= temperature, °R
u	= x component of velocity
v	= y component of velocity
v_w	= vaporization velocity
$v_{-\infty}$	= ablation velocity
x	= coordinate along body surface
y	= coordinate normal to body surface
W	= body weight
W/C_{DA}	= ballistic missile parameter
α	= optical coefficient, ft^{-1}
δ	= liquid layer thickness
δ_T	= thermal thickness, $\delta_T = n\delta$
θ	= angle generated by rotation of nose radius away from stagnation point
ϵ	= emissivity
λ	= effective radiation mean free path
μ	= viscosity
ρ	= density
σ	= Stefan-Boltzmann constant
τ	= shear stress
τ_0	= shear stress on nonablating surface
ψ	= ratio of heat transfer rates with to without mass injection

Subscripts

a	= absorption
i	= liquid-gas interface
L	= liquid

r	= radiation
s	= scattering
T	= thermal
v	= property of glass vapor
x	= differentiation with respect to x
w	= liquid-gas interface
∞	= liquid-solid interface

THE ablation process consists of the melting and vaporization of the surface material of a body that re-enters the atmosphere at hypersonic speeds. For a glassy material such as quartz, this process is described physically by an incompressible, highly viscous liquid layer immediately underneath the air boundary layer. A steady-state theory for this ablation process has been developed for both laminar and turbulent heating (1-3).⁴ This theory matches the solution of the equations of motion for the radiating liquid layer with vaporization at the liquid-gas interface to the solution of the air boundary layer equations with mass injection from the vaporization. The solution of the liquid layer is obtained by neglecting the inertia terms in the momentum equation (1,4) and using conventional integral methods. The gas boundary layer is solved numerically (2,5,6) when it is laminar and empirically (2,7,8) when it is turbulent. The basic aerodynamic parameters such as pressure distribution around the body, heat transfer rates, shear forces without mass injection, and transition from laminar to turbulent flow in the boundary layer have been studied in Refs. 9-20. The foregoing ablation theory was verified experimentally in the arc wind tunnel for conditions of stagnation point laminar heating (21). However, it was not possible to do so for the important case of turbulent heating because of power limitations in arc wind tunnel development. It is therefore of great interest to use flight ablation data for a complete evaluation of this theory.

A full-scale experiment was performed by flying a nose cone along a typical 5000-naut mile trajectory and recovering it after flight. The missile geometry is of the Thor-Able type (2), which consists of a spherical nose, followed by a cone, a cylinder, and a skirt. The ablation material on the spherical nose and cone was opaque quartz (21). The ablation theory is evaluated by comparing theoretical and experimental values for the ablation thickness around the spherical nose and cone, the weight loss of material from the nose cap and cone, and the vaporized material during re-entry, which is measurable from the recondensed ablated material on the forward section of the cylinder.

Ablation Theory

Ref. 2 presents a theory for the steady-state ablation of glassy materials under both laminar and turbulent heating,

Received by ARS January 22, 1962; revised July 10, 1962.

¹ This work was supported by Headquarters, Ballistic System Division, Air Force Systems Command, U. S. Air Force, under Contract No. AF 04(647)-278.

² Formerly Principal Research Engineer; presently with Heliodyne Corporation, West Los Angeles, Calif. Senior Member ARS.

³ Consultant.

⁴ Numbers in parentheses indicate References at end of paper.

Table 1 Optical constants of opaque quartz^a

Constant	Symbol	Value	Error
Refractive index	\hat{n}	1.5	± 0.1
Effective surface reflectivity for internally produced radiation	R_{eff}	0.2	± 0.2
Effective radiation mean free path	$\lambda \equiv 1/\alpha$	2.4×10^{-3} ft	$\pm 0.7 \times 10^{-3}$ ft
Ratio of effective radiation mean free path to mean free path between absorptions	α_a/α	0.15	± 0.03
Ratio of scattering mean free path to absorptions mean free path	α_s/α_s	0.07	± 0.03

^a For detailed explanation of the meaning of these constants, see Ref. 23.

including radiation effects from the high temperature ablating material. The energy equation for the liquid layer yields the following result:

$$q_i - \epsilon \sigma T_w^4 = (1 + \xi) \rho c_p v_{-\infty} T_w \quad [1]$$

where

$$q_i = \psi q_0 - \rho v_w h_v \quad [1a]$$

$$\xi = \xi_1 - \xi_2 \quad [1b]$$

$$\xi_1 = \frac{1}{v_{-\infty} T_w} \left[\int_{-\infty}^0 u T_x dy - \frac{1}{r} \int_{-\infty}^0 T_y \left(r \int_{-\infty}^y u dy \right)_x dy \right] \quad [1c]$$

$$\xi_2 = \frac{1}{\rho c_p v_{-\infty} T_w} \int_{-\infty}^0 (u p_x + \mu u_y^2) dy \quad [1d]$$

Eq. [1] relates the ablation temperature T_w to the ablation velocity $v_{-\infty}$. The heat transfer rate at the liquid-gas interface q_i is determined from the aerodynamic heat transfer rate with mass injection (ψq_0) as reduced by the energy necessary to vaporize the ablating material that is injected into the gas boundary layer ($\rho v_w h_v$). The function ψ is unity for zero mass injection; otherwise it is reduced by a term that depends on the nature of the heating rates (laminar or turbulent). The integrals in Eqs. [1c] and [1d] are evaluated in Ref. 2. The energy equation [1] can also be used to define the effective energy of ablation h_{eff} as follows:

$$h_{\text{eff}} \equiv \frac{q_0}{\rho v_{-\infty}} = (1 + \xi) c_p T_w + \frac{v_w}{v_{-\infty}} h_v + (1 - \psi) h_{\text{eff}} + \frac{q_r}{q_0} h_{\text{eff}} \quad [1e]$$

The four terms on the right-hand side of Eq. [1e] represent, respectively, the mechanisms of heat absorption by conduction into the ablating body, vaporization of the ablated material, mass injection effect of vaporized material into the gas boundary layer, and the energy that is radiated away from the ablating body.⁵ This theory gave the important result that, in the ablation of quartz under turbulent heat transfer conditions, the fraction of vaporization $v_w/v_{-\infty}$ increases significantly from the laminar value (2).

The solutions of the continuity and momentum equations in the liquid layer yield the following result:

$$\frac{v_w}{v_{-\infty}} = 1 - \frac{1}{r v_{-\infty}} \frac{d}{dx} \left[r \left(\frac{\tau_w \delta^2}{\mu_w} - \frac{2 P_x \delta^3}{\mu_w} \right) \right] \quad [2]$$

where

$$\mu \propto \exp[124,000/T(^{\circ}\text{R})] \quad [2a]$$

$$\delta_{\lambda/\delta} < 1 = \frac{k}{(1 + \xi) \rho c_p v_{-\infty}} \quad [2b]$$

⁵ An additional process of heat absorption is present when the ablating material reacts chemically with the air boundary layer. It can be shown, however, that for quartz this effect is negligibly small.

$$\delta_{\lambda/\delta} > 1 = \frac{k}{(1 + \xi) \rho c_p v_{-\infty}} \times \frac{1}{1 + [\epsilon \sigma T_w^4 / (1 + \xi) \rho c_p v_{-\infty} T_w]} \quad [2c]$$

The vaporization velocity v_w is determined from the diffusion process in the gas boundary layer. Hence, Eq. [2] is a linear differential equation for the ablation velocity and is coupled to Eq. [1] through the ablation temperature. Eq. [2a] defines the viscosity for uncontaminated quartz (22). Eqs. [2b] and [2c] show the effect of radiation mean free path on the liquid layer thickness and therefore on the ablation velocity. The integration of the momentum equation in the liquid layer uses the expression

$$\mu = \mu_w e^{-y/\delta} \quad [2d]$$

where δ is a function of x and is determined from the energy equation. The foregoing expression implies also a temperature distribution through the liquid layer, because Eq. [2a] may be expressed in a small temperature range as

$$\mu = \mu_w (T/T_w)^{-n} \quad [2e]$$

where n is a function of temperature but may be considered to be constant in a small temperature range. (This result is obtained by matching slopes and viscosity levels from [2a] and [2c].) Hence, these expressions yield

$$T = T_w e^{y/n\delta} = T_w e^{y/\delta_T} \quad [2f]$$

This result is used in the integration of the energy equation and in the determination of the emissivity of the uncontaminated ablation material, as is shown in the following section.

Emissivity of Opaque Quartz

From the foregoing equations, it is seen that the emissivity of the ablation material has a strong effect on the liquid layer

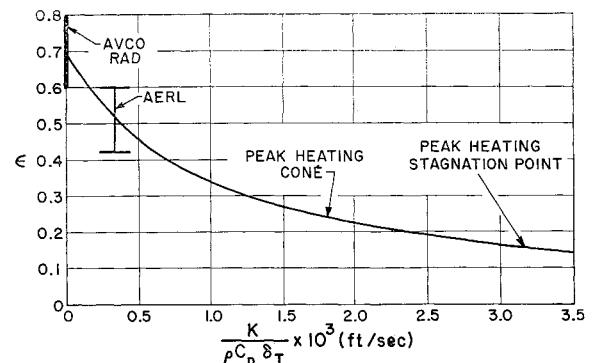


Fig. 1 Emissivity as a function of thermal thickness. The AVCO-RAD data represent measurements of the emissivity of a large nonablating slab of opaque quartz. The AERL data represent measurements of emissivity in the Avco-Everett Research Laboratory arc wind tunnel

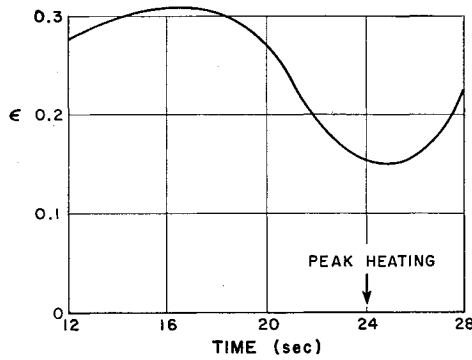


Fig. 2 Variation during re-entry of the calculated emissivity at the stagnation point of body used in present flight

thickness, the ablation temperature, and the ablation velocity. It has also an effect on the temperature distribution within the ablating body (23). The emissivity is evaluated from the flux of radiation, which, for a semi-infinite slab that can emit, absorb, and scatter radiation, is given by (23)

$$q_r = (1 - R_{eff}) \int_{-\infty}^0 2\alpha_a \hat{n}^2 \sigma T^4(y) e^{\alpha y} dy \quad [3]$$

This equation is based on the fact that an element of volume between y and $y + dy$ produces a flux of radiation $2\alpha_a \hat{n}^2 \sigma T^4$ that is attenuated by $e^{\alpha y}$ while traveling to the surface. (Here, α^{-1} acts as an effective radiation mean free path.) The beam is further attenuated at the surface by the factor $(1 - R_{eff})$.

Using Eq. [2f] in [3], one obtains the following result:

$$\epsilon = \frac{2\alpha_a \hat{n}^2}{\alpha} \frac{1 - R_{eff}}{1 + 4/\alpha n \delta} \quad [3a]$$

The optical constants of opaque quartz have been measured in the laboratory at the Avco Research and Advanced Development Division. The results are shown in Table 1. With these tabulated values, Eq. [3a] becomes

$$\epsilon = \frac{0.7}{1 + 10^{-2}/n\delta} = \frac{0.7}{1 + 10^{-2}/\delta_T} \quad [3b]$$

where δ is given in feet. This expression shows the dependence of emissivity on the thermal layer thickness δ_T , which is defined as the thickness necessary for the temperature to drop by a factor of $1/e$. This thickness is larger than the liquid layer thickness because $n \gg 1$. The reason for the foregoing dependence is that, for a semitransparent

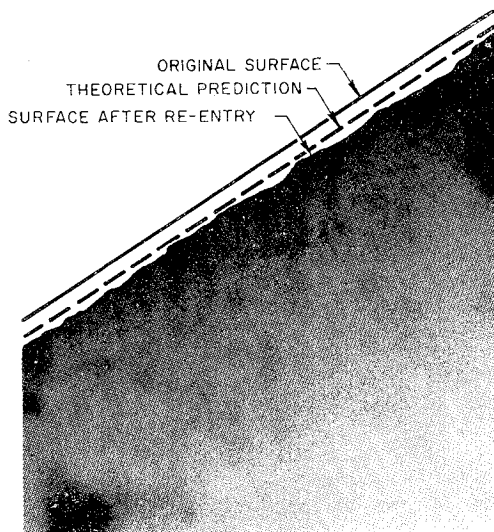


Fig. 3 Section of pre-launch, recovered, and calculated nose cone profiles

Table 2 Physical properties of quartz (Ref. 2)

Heat of vaporization, Btu/lb	5500
Density, lb/ft ³	140
Specific heat, Btu/lb-°R	0.25
Thermal conductivity, Btu/ft-sec-°R	3.2×10^{-4} , $T > 1800^\circ\text{R}$
Viscosity, lb/ft-sec:	$\mu = 0.0672 \exp[124,000/T(^{\circ}\text{R}) - 20]$
Vapor pressure law:	$(p_v/p_v^*)[0.4 + 0.6(p/p_v)]^{1/3} = 1;$ $p_v^* = \exp[-104,000/T(^{\circ}\text{R}) + 18.48]$

material such as opaque quartz, the emission of radiation is a volume and not a surface effect. If the thermal layer is large, the amount of hot material is also large, and the emissivity will be high. This is an important consideration in the application of arc wind tunnel measurements of emissivity to actual flight conditions.

Eq. [3b] is plotted in Fig. 1, which shows also a comparison of theory with experimental measurements of emissivity at low ablation velocities or high thermal thicknesses. The point at $\delta_T \approx \infty$ is a measurement by C. Leigh of the Avco Research and Advanced Development Division, who used a nonablating slab of opaque quartz placed in a furnace. (Here δ_T is very large, effectively equal to the body dimensions of the slab.) The other experimental point is a measurement by M. Camac in the Avco-Everett Research Laboratory arc wind tunnel. The figure also shows the calculated emissivity at peak heating conditions for the recovered nose cone described earlier. The variation of emissivity at the stagnation point during re-entry is indicated in Fig. 2, and it is based on a thermal thickness obtained from a nonsteady-state ablation analysis (24) with $\epsilon = 0.25$. This figure indicates that a mean value for the emissivity at the stagnation point during re-entry is $\epsilon = 0.25$.

Flight Experiment

The steady-state ablation theory (2) was applied to the geometry and trajectory of this flight with a constant emissivity value of $\epsilon = 0.25$ and the constants in Table 2. The expression for a transparent liquid layer was used because $\lambda/\delta \gg 1$. For example, at conditions near peak heating, $\delta \approx 2 \times 10^{-4}$ ft near the stagnation point. From Table 1, $\lambda = \alpha^{-1} = 24 \times 10^{-4}$. Hence, $\lambda/\delta = 12$.

Results

Fig. 3 shows a section of the body profile before flight together with the actual and theoretical body contours after the flight. (When scales are omitted, it is because of classification requirements.) Fig. 4 presents a relative comparison of the flight and calculated results for the ablated thickness or change in body contour after re-entry. At a given loca-

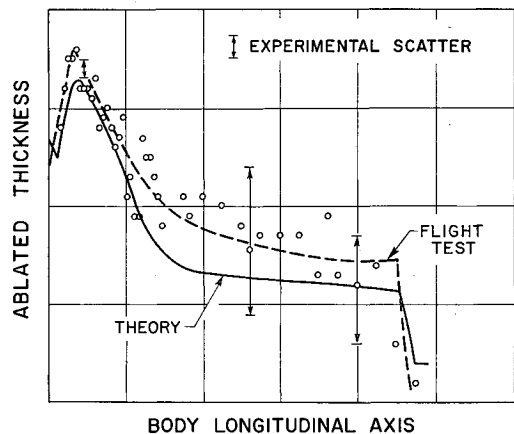


Fig. 4 Relative comparison of ablated thickness from flight data and steady-state theory

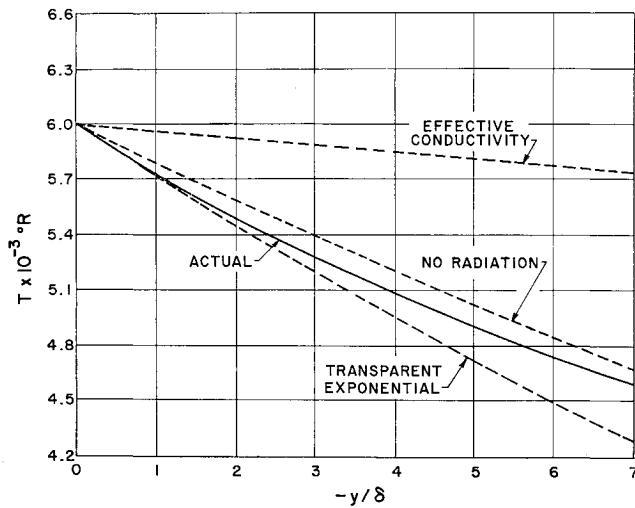


Fig. 5 Temperature vs distance from wall for steady-state ablation. The wall temperature and the ablation velocity are chosen for conditions near peak heating at the stagnation point. The "actual" temperature includes radiative effects (23), whereas the other curves represent possible approximations for this temperature

tion along the surface of the body, the ablated thickness is a function of angular position because of the waviness of the surface of the recovered nose cone (Fig. 3). The points represent the average of the ablation around the 360° at each cross section perpendicular to the longitudinal axis of the nose cone. The arrows indicate the scatter produced by the waviness of the surface. The error in the average values is estimated to be about one half the size of the scatter. The dashed line is a mean line drawn through the points. From these data, it is found that the theoretical and flight values for ablation thickness agree to within 10% on the spherical nose and between zero and 30% on the cone. This latter value is, however, of the same magnitude as the scatter of the data on the cone. For the loss of ablated material from the spherical nose and cone, the agreement between theory and flight values is to within 20%.

A further test of the ablation theory is obtained from the comparison of flight and theoretical values for the vaporized

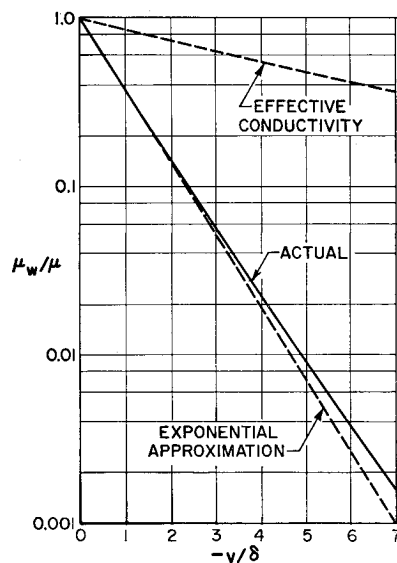


Fig. 6 Viscosity vs distance from wall. The "actual" and "effective" conductivity lines are computed from the corresponding temperature distribution in Fig. 5. The exponential approximation is computed from the transparent temperature distribution

Table 3

	Frozen, ablated	Vaporized, ablated
Flight	0.41	0.59
Theory	0.43	0.57

material during re-entry. At the cylindrical section of the body immediately behind the cone, the heat transfer rates decrease because of the Prandtl-Meyer expansion and further pressure decay along the cylinder (17,19). Hence, as the highly viscous liquid layer flows on to the cylinder, the liquid condenses back to the solid state. From the weight of this recondensed material and the weight loss from the sphere and cone sections, it is possible to obtain an experimental value for the fraction of vaporized material. The results are given in Table 3 and show excellent agreement for the vaporized material during re-entry. The small errors in the ablation thickness can be attributed to the lack of precise knowledge concerning the viscosity and emissivity of the ablative material.

Accuracy of the Viscosity of Flight Material

The ablative material on the nose cone contains a structural honeycomb that is dissolved during ablation and thus modifies the viscosity of the opaque quartz. Experiments in the arc wind tunnel indicate that the honeycomb material increases the ablation thickness by about 20%. These results are based on experiments with opaque quartz specimen with and without the honeycomb material. Since the theory uses a viscosity law for quartz without the honeycomb material, this becomes a main source of error in the theoretical results. Also, the viscosity of quartz without the honeycomb material is not well known at high temperature. Eq. [2a] has not been verified at the high ablation temperatures, but it has been shown that, when the viscosity values from Eq. [2a] are varied arbitrarily by a factor of ± 3.0 , the corresponding ablation thicknesses change only by $\pm 20\%$ (2).

There are no significant errors introduced in the theoretical results from the use of the exponential viscosity distribution, Eq. [2d]. This result is obtained by comparing it with the exact viscosity distribution as obtained from an exact temperature distribution (23) together with Eq. [2a]. Fig. 5 shows the exact temperature distribution for conditions near peak heating at the stagnation point of the nose cone and compares it with the exponential temperature distribution, Eq. [2f], for both the opaque and transparent liquid layers, i.e., Eqs. [2b] and [2c], respectively. (As a matter of interest, a temperature distribution from the well-known concept of effective conductivity (23) is also included to show its poor accuracy.) It is seen that in the region of maximum

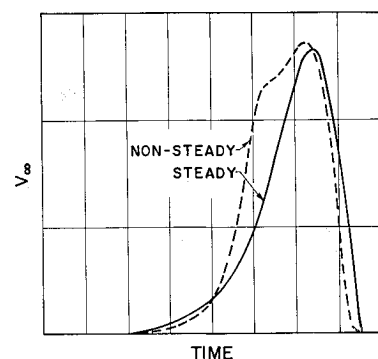


Fig. 7 Relative comparison of steady- and nonsteady-state ablation velocities at stagnation point during re-entry

flow ($0 < -y/\delta < 2$) the transparent exponential approximation is quite accurate for the temperature and therefore the viscosity (Fig. 6). This is a somewhat general result because the liquid layer is usually transparent to radiation.

Accuracy of the Emissivity

Eq. [3b] for the emissivity has small errors because of inaccuracies in the optical constants and the use of an exponential rather than the exact temperature distribution. These factors indicate that for this flight the emissivity has a value of $\epsilon = 0.25 \pm 0.1$ during the times of appreciable ablation. Ref. 2 shows the effect of emissivity on ablation thickness. The ± 0.1 uncertainty in emissivity produces an uncertainty in ablated thickness of the order of $\pm 10\%$.

Effect of Unsteady-State Ablation

Nonsteady effects in the liquid layer are introduced only through the term $\partial T/\partial t$ in the energy equation. The continuity and momentum equations are unaffected because of the incompressibility of the liquid and the smallness of the inertia forces as compared with the viscous forces. This unsteady effect has been considered for the conditions of zero radiation (24), but its extension to the radiation case is straightforward with an exponential temperature distribution. Fig. 7 shows a relative comparison for the steady and unsteady ablation velocities at the stagnation point for this flight case. It is found that, although the time history of the ablation velocities can be somewhat different, the total ablated thickness or area under the curves is about the same for steady and unsteady ablation. Hence, the effect does not introduce significant errors in the results for ablation thickness from the steady state-theory.

Other Effects

It is believed that there are no other sources of errors comparable in magnitude to the foregoing effects of viscosity and emissivity. The trajectory was calculated from accurate knowledge of the $W/C_D A$ parameter and re-entry conditions. The effect of angle of attack or oscillatory motion of the body on the heating rates was neglected because these angles are usually small in the initial phase of significant aerodynamic heating. The turbulent heat transfer rates without mass injection have been verified from shock tube experiments (15,16), and mass injection does not reduce the turbulent heat transfer rates so effectively, as in the case of laminar boundary layers, which are better known.

Conclusions

The steady-state ablation theory for glassy materials, as reported in Ref. 2, predicts very accurately the ablation of opaque quartz under both laminar and turbulent heating, as is confirmed from flight measurements of time integrals

of ablation velocity, and a double integration with respect to time and space of the vaporization and ablation velocities.

Acknowledgments

The authors wish to thank J. B. Lopez of the Avco Research and Advanced Development Division, Wilmington, for his explanation of the measurements of the ablated distances along the surface of the nose cone; and Michael Gattozzi of Avco-Everett Research Laboratory for doing the IBM computations.

References

- 1 Bethe, H. A. and Adams, M. C., "A theory for the ablation of glassy materials," *J. Aero/Space Sci.* **26**, 321-328 (1959).
- 2 Hidalgo, H., "Ablation of glassy materials around blunt bodies of revolution," Avco-Everett Research Lab. Research Rept. 62 (June 1959); also ARS J. **30**, 806-814 (1960).
- 3 Bethe, H. A. and Adams, M. C., "On the accuracy of an approximate theory for the ablation of glassy materials—A reply," *J. Aero/Space Sci.* **26**, 768 (1959).
- 4 Lees, L., "Similarity parameters for surface melting of a blunt nosed body in a high velocity gas stream," *ARS J.* **29**, 345-354 (1959).
- 5 Baron, J. R., "The binary mixture boundary layer associated with mass transfer cooling at high speeds," *Mass. Inst. Tech. Naval Supersonic Lab. TR 160* (May 1956).
- 6 Reshotko, E. and Cohen, C. B., "Heat transfer at the forward stagnation point on blunt bodies," *NACA TN 3513* (July 1955).
- 7 Rubesin, M. W., Pappas, C. C., and Okuno, A. F., "The effect of fluid injection on the compressible turbulent boundary layer—Preliminary tests on transpiration cooling of a flat plate at $M = 2.7$ with air as the injected gas," *NACA TN A55119* (December 1955).
- 8 Pappas, C. C. and Okuno, A. F., "Measurements of skin friction of the compressible turbulent boundary layer on a cone with foreign gas injection," *J. Aero/Space Sci.* **27**, 321-333 (1960).
- 9 Lees, L., "Laminar heat transfer over blunt nosed bodies at hypersonic flight speeds," *Jet Propulsion* **26**, 259-269 (1956).
- 10 Fay, J. A. and Riddell, F. R., "Theory of stagnation point heat transfer in dissociated air," *J. Aeronaut. Sci.* **25**, 73-85 (1958).
- 11 Kemp, N. H., Rose, P. H., and Detra, R. W., "Laminar heat transfer around blunt bodies in dissociated air," *J. Aero/Space Sci.* **26**, 421-430 (1959).
- 12 Rose, P. H., Probst, R. F., and Adams, M. C., "Turbulent heat transfer through a highly cooled partially dissociated boundary layer," *J. Aero/Space Sci.* **25**, 751-760 (1958).
- 13 Van Driest, E. R., "Turbulent boundary layer in compressible fluids," *J. Aeronaut. Sci.* **18**, 145 (1951).
- 14 Hidalgo, H., "On the application of Van Driest method to a highly cooled partially dissociated turbulent boundary layer," *Jet Propulsion* **28**, 487-488 (1958).
- 15 Offenhartz, E. and Weisblatt, H., "Experimental determination of the turbulent heat transfer rate distribution along a slender blunt nosed body from shock tube tests," *RAD-TR-9-59-18*, Research and Advanced Dev. Div., Avco Corp., Wilmington, Mass. (May 1959).
- 16 Hidalgo, H., "Closing reply," *ARS J.* **32**, 647-648 (1962).
- 17 Detra, R. W. and Hidalgo, H., "Generalized heat transfer formulas and graphs for nose cone re-entry into the atmosphere," *ARS J.* **31**, 318-321 (1961).
- 18 Stetson, K. F., "Boundary layer transition with highly cooled boundary layers," *J. Aero/Space Sci.* **27**, 81-91 (1960).
- 19 Feldman, S., "Numerical comparison between exact and approximate theories of hypersonic inviscid flow past slender blunt nosed bodies," *ARS J.* **30**, 463-468 (1960).
- 20 Cheng, K. H. and Chang, A. L., "On 'Numerical comparison between exact and approximate theories of hypersonic inviscid flow past slender blunt nosed bodies'," *ARS J.* **31**, 1024-1026 (1961).
- 21 Adams, M. C., Powers, W. E., and Georgiev, S., "An experimental and theoretical study of quartz ablation at the stagnation point," *J. Aero/Space Sci.* **27**, 535-543 (1960).
- 22 "Properties of selected commercial glasses," *Corning Glass Works Bull. B-83*, Corning, N. Y. (1957).
- 23 Kadanoff, L. P., "Radiative transport within an ablating body," *J. Heat Transfer* **83**, 215-224 (1961); also Avco-Everett Research Lab. Note 61 (July 1959).
- 24 Georgiev, S., "Unsteady ablation," Avco-Everett Research Lab. Research Rept. 94 (September 1959).